Contents list available at: https://journals.ekb.eg/
Sohag Journal of junior Scientific Researchers
journal homepage: https://sjyr.journals.ekb.eg/
ISSN 2735-5543

Article

Characterization of vanadium oxide thin films for optoelectronic application

E. Kh Shokr[1]*, H. A Mohamed[1], Sh. A. Elkot[1]*, H. M. Ali[1]

[1]Department of Physics, Faculty of Science, Sohag University, Sohag 82524, Egypt.

*Correspondence: nasrshaimaa2@gmail.com

Article info

Citation: Shokr, E., Kh.; Mohamed, H., A.; Ali, M. H.,

Title. Characterization of vanadium oxide thin films for optoelectronic application *SJYR* **2024**, *4*,(2), 13-26. 10.21608/SJYR.2024.262806.1407

Academic Editor: Mohamed Kelany

Received: 31/05/2024
Accepted: 25/09/2024
Published: 29/09/2024

Publisher's Note: SJYR stays neutral with regard to jurisdictional claims in published maps and institutional affiliations.

Abstract

Monoclinic V_2O_3 thin films with 558 and 620 nm thick were deposited by spin coating of viscous vanadium oxide sol-gel on glass and single crystal Silicon (Si) substrates. The crystallographic structure, surface morphology, and optical and thermoelectric properties were examined and discussed. V_2O_3 films have high surface homogeneity. The direct optical band gap energy and the localized state width of these samples were depicted to be 1.82-1.8 eV and 1.98-2.4 eV respectively, the free carrier concentration increases from 2.44 x 10^{21} to 4.42 x 10^{21} cm^{-3} by increasing the film thickness. The relatively high average values of absorption coefficient 1.16×10^4 cm^{-1} in the visible spectral range, besides the positive Seebeck coefficient (104.3 μV/℃) for the film of 620 nm thick qualify this sample to be used as an absorber layer un thin-film solar cells. In this work, the solar cell with the structure ITO/CdS/V_2O_3/Mo/Glass has been accomplished. It was found that the short circuit current density (J_{sc}) and the solar cell efficiency (η) in the absence of optical and recombination losses are 19.4(mA/cm^2) and 14.68 %, respectively. When the optical losses are taken into consideration, J_{sc} and η recorded the values of 13.3(mA/cm^2) and 9.6 %, respectively. Finaly when both the optical and recombination losses were affected in the cell, the values of J_{sc} and η decreased and reached to 6.23 (mA/cm^2) and 4.2 %, respectively.

Keywords: vanadium oxide thin films; sol-gel; spin coating; optical and electrical properties; solar cells.

1. Introduction:

Vanadium oxide thin films are one of the most important transition metal oxide semiconductors due to their unique properties such as high chemical stability, electrochemical safety, low cost, easy preparation, and relatively low toxicity (Alamgir et al., 2014: Raj et al., 2013: Raja et al., 2016: Zou et al., 2010).

The used technique in the deposition of vanadium oxide thin films has a high effect on their structure and morphology properties (Mouratis et al., 2020). Various physical and chemical vapor deposition techniques have been used to deposit Vanadium oxide thin films, one of them is the sol-gel technique (Alamgir et al., 2014: Raj et al., 2013: Gao et al., 2005), where V_2O_{5-x} thin films could be prepared from gels using either spin-coating (Benmouss et al., 2003: Ozer& Lampert, 1999: Özer N, 1997: Shimizu et al., 1990: Nagase et al., 1992) or dip-coating (Partlow et al., 1991: Hirashima& Sudoh, 1992: El Mandouh& Selim, 2000) methods.

Vanadium oxides can form four single valence oxides from V^{2+} and V^{5+}, in the form of VO, V_2O_3, VO_2, and V_2O_5, due to the variability of oxygen coordination geometries. However, vanadium-oxygen phases can also consist of mixed oxidation states formed due to the presence of oxygen vacancies in the oxides of the mentioned higher oxygen index (Huotari, 2018). When the density of these vacancies becomes high enough along the lattice planes, the so-called crystallographic shear planes are formed leading to eliminating the effects of vacancies (Henrich& Cox, 1994). This changes the crystal structure of the compound into mixed stoichiometry oxides, such as the Magnéli phases with VnO_{2n-1}, or the Wadsley phases with $V_{2n}O_{5n-2}$ (Pedrosa et al., 2017: Surnev et al., 2003).

This unique structure of vanadium oxide thin films gives their optical properties several advantages, which makes them suitable for various applications (Ali& Hakeem, 2015: Atuchin et al., 2008) such as electrochromic devices (Tong et al., 2016), electro-optic switches (Wang et al., 2005), CdTe solar cell with V_2O_5 as a back contact buffer layer (Tong et al., 2016), a window for solar cells, color filters (Atuchin et al., 2008), reflectance mirrors, smart windows, surfaces with tunable emittance for temperature control of space vehicles (Shen et al., 2016: Ramana et al., 1998: Park et al., 2002: Wu Q-H et al., 2004), and cathode material of Lithium-ion rechargeable batteries (Pan et al., 2016: Song et al., 2015: Ihsan et al., 2015: Niu et al., 2015: Sel et al., 2014).

In this work, the optical and thermoelectric properties of vanadium oxide thin films of relatively high thickness (558 & 620 nm) deposited on glass substrates by sol-gel spin coating will be studied and examine these samples to be used as a p-type conductive layer in solar cell applications.

2. Experimental:

2.1. Thin film preparation:

V_2O_3 thin films with thicknesses of 558 and 620 nm were deposited on glass substrates and 620 nm on Si-sheets by sol–gel spin coating method. 0.5 g V_2O_5 powder of 99.5% purity was dissolved in 30 ml of 15% H_2O_2 solution under vigorous agitation (1000 rpm) until the solution color changed from orange to red-brownish. After heat treatment in a water bath at 80^o C for 30 min the solution transformed into a viscous solution forming V_2O_3 gel.

The viscosity of the gel can be controlled through the water bath temperature and heating time. The films were deposited on glass and single crystal silicon (Si) substrates which were highly cleaned by rinsing them in a heated solution of both acetone and distilled water in an ultrasonic cleaner instrument (VGT-1613 QTD) with a capacity of 2000 mL and provided with

digital timer. A suitable portion of the gel was spin-coated on glass and Si substrates at a suitable speed of 1000 to 1200 rpm depending on the required film thickness. The samples were annealed in air at 150 ^{0}C for 1 hour for drying.

The weigh method was used to determine the deposited film thicknesses according to the following equation (Libessart et al., 2014):

$$d(nm) = \frac{m}{\rho\, A} \times 10^7 \qquad (1)$$

where, m is the film mass (gm), ρ (g.cm^{-3}) is vanadium oxide density, and A is the film area (1.5x 3.2 cm^2).

2.2. Investigation techniques

The crystallographic structure of the samples deposited on glass substrates was examined by using X-ray diffractometer (XRD) type Philips (model PW1710) with a Cu - target and K_α - filter, λ=1.541838A^0 in the range of 2θ from 10 to 80^0. The x-ray diffractometer works at 40 kV and 30 mA with a scanning speed of 2^o/min.

The surface morphology of the films has been checked by field-emission scanning electron microscopy (FE-SEM) using a JSM-6100 microscope with an acceleration voltage of 30 kV. The chemical composition of the films deposited on Si-substrates was analyzed using energy dispersive analysis of x-ray (EDAX) unit attached with the FE-SEM (EDS unit, HNU-5000).

The optical absorption A, and the reflection R spectra for the samples deposited on glass substrates were recorded at RT using a computer-programmable double beam spectrophotometer model Jasco-570 with reflectivity attachment model ISN-470 (Japan) at normal incidence with a scan speed of 400 nm/min in the wavelength range of 200- 2500 nm. These optical measurements were used to determine different important absorption, dielectric and dispersion parameters such as the absorption coefficient α , the extinction coefficient k, and the refractive index n according to the following equations (Rusop et al, 2006: Mohamed& Ali, 2008);

$$Abs. = \alpha d = 2.303 \log\left[\frac{(1-R)^2}{T}\right] \qquad (2)$$

$$n = \left(\frac{1+R}{1-R}\right) + \left[\left(\frac{1+R}{1-R}\right)^2 - (1+K^2)\right]^{\frac{1}{2}} \qquad (3)$$

$$\& \;\; K = \alpha\lambda/4\pi \qquad (4)$$

, where Abs. is the absorbance and d is the film thickness.

Seebeck coefficient of V_2O_3 films was measured at room temperature to identify the conductivity type and majority carriers, its calculated using the following equation (Wang et al., 2012);

$$S = \Delta V/\Delta T \qquad (5)$$

, where S is Seebeck coefficient which is the value of the developed electromotive force between the two ends of the thin film when the temperature difference ΔT. The developed electromotive force and the temperature were recorded by means of microvoltmeter and thermal contact chromel-alumel thermocouple, respectively**.**

3. Results and discussion:

3.1 Structural and surface morphology analyses:

Figure 1 depicts the XRD diffractogram of V_2O_3 thin films which reveal three weak peaks only at 2θ = 24.963, 33.275 and 41.685^0 assigned to the monoclinic V_2O_3 (embedded in a highly amorphous matrix) with lattice parameters a= 8.6 A^0, b= 5.002 A^0, c= 7.255 A^0 and β = 140.17^0 according to the JCPDS file (card number 96-153-9771) (Long et al., 2018). This monoclinic structure refers to the film oxygen deficiency (V_2O_{5-x}), where x= 2 (Alamgir et al., 2014: Raj et al., 2013: Gao et al., 2005) leading to the formation of V^{3+} instead of V^{5+}.

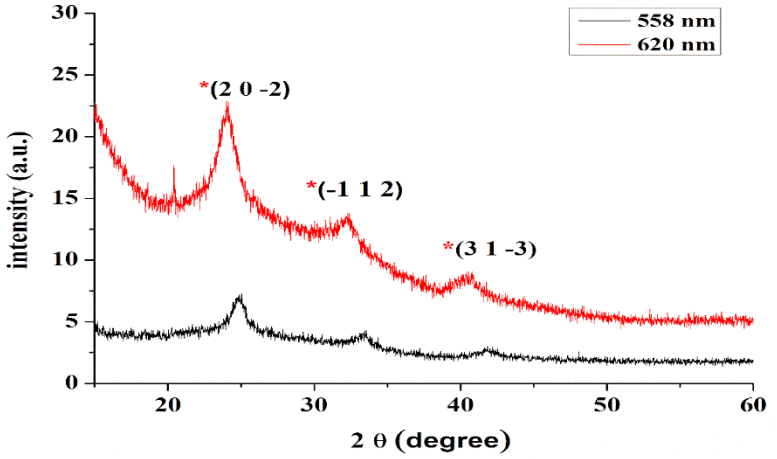

Figure 1: XRD diffractogram of V_2O_3 thin films deposited on glass substrates.

The crystallite sizes of V_2O_3 thin films were calculated by using the FWHM of the preferred crystallization (2 0 -2) peaks using Debye Scherrer's formula (Subramanian& Padiyan, 2008: Benramdane et al., 1997).

$$D = \frac{0.9\,\lambda}{\beta\, COS\,\theta} \qquad (6)$$

where D is the grain size, λ is the used X-ray wavelength, β is the angular line width at half-maximum intensity in radians and θ is Bragg's angle. The dislocation density (δ) which referring to the number of defects in the films can depicted using the following formula (Subramanian& Padiyan, 2008: Benramdane et al., 1997);

$$\delta = \frac{1}{D^2} \qquad (7)$$

, and the number of crystallites per unite area given by the following equation (Subramanian& Padiyan, 2008: Benramdane et al., 1997):

$$N = \frac{d}{D^3} \qquad (8)$$

, where d is the film thickness.

The calculated D, δ and N values are listed in table 1. Due to the decreases in the FWHM of the preferred orientation of crystallization according to (2 0 -2) peak, the crystallite size D increases by increasing the film thickness. Accordingly, the dislocation density δ and the number of crystallites N decrease by increasing the film thickness as expected by equations 7 & 8, respectively.

Table 1: The crystallite size D, dislocation density δ and number of crystals per unit area of V_2O_3 thin films.

Film thickness, d, nm	FWHM (rad.)	crystallites size D, nm	dislocation density δ, nm^{-2}	number of crystallites N, nm^{-2}
558	0.0164	8.647	0.0134	0.86
620	0.014	9.677	0.0107	0.68

The surface topography of the as deposited films of 558 and 620 nm thick shown in Figure 2 which illustrates the high sample surface homogeneity with clear grains shape, and their size in micro-meter scale.

The EDAX analyses for V_2O_3 film of 620 nm thick deposited on single crystal Si substrates depicted in Figure. 3, where the films are composed only of V, and O. The O/V ratio calculated by the EDAX- data was found ≈ 1.5. This indicates that the formula V_2O_{5-x} corresponds to the V_2O_3 – compound referring to the presence of oxygen vacancies due to the oxygen deficiency, this matching with X-ray analysis.

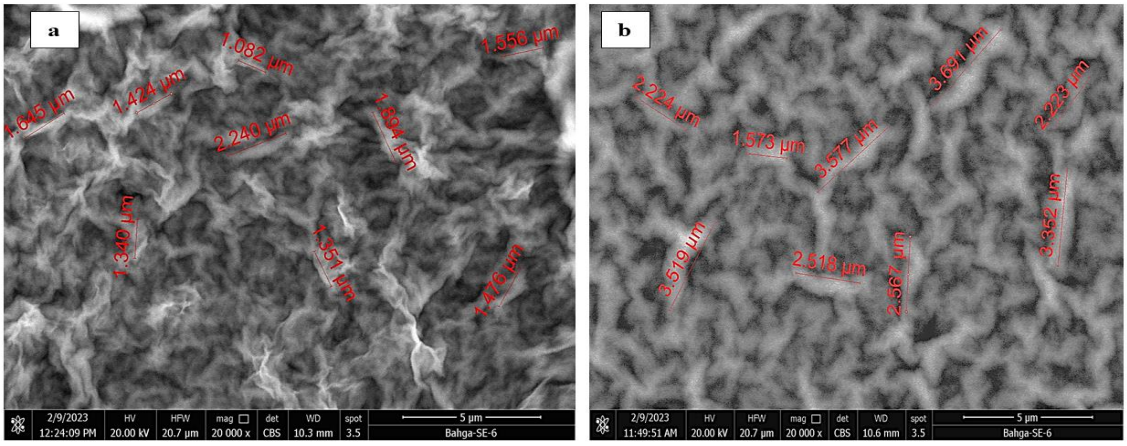

Figure 2: SEM morphology analysis of V_2O_3 thin films on glass substrates with thicknesses (a) 558 nm, and (b) 620 nm.

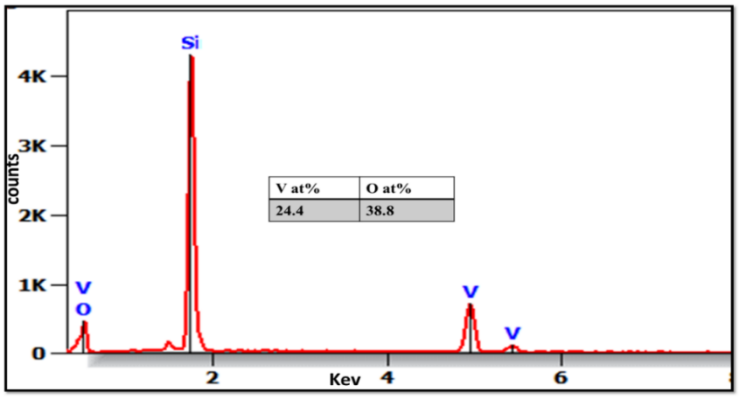

Figure 3: EDAX analysis of V_2O_3 thin film of 620 nm thick deposited on Si substrate.

3.2 The optical properties:

Figure 4 gives the optical absorption (A) and reflection (R) spectra of the present vanadium oxide thin films. by increasing the film thickness from 550 to 620 nm A increases but R decreases and the absorption band edge shifts towards higher wavelength values, indicating the decrease of the optical band gap energy with film thickness increase.

The absorption coefficient (α) can be given by the following Tauc equation (Saleh et al., 2014),

$$\alpha h\upsilon = \beta(h\upsilon - E_g)^{1/r} \qquad (9)$$

where β is a constant, E_g is the optical band gap energy, r is a number that characterizes the type of electron transition, where r is equal to 1/2 or 2 for allowed indirect or direct transitions, and 3, 3/2 for forbidden direct and indirect transitions, respectively. Where, Tauc equation is satisfied only at r = 2 which corresponding to the direct allowed transition.

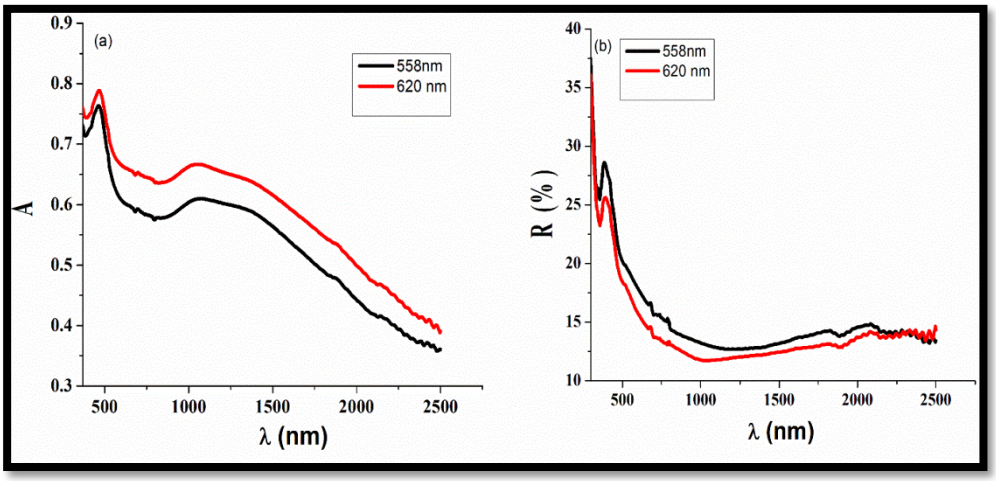

Figure 4: the optical absorption (a) and reflection (b) spectra of V_2O_3 thin films of 558 and 620 nm thick deposited on glass substrates.

Figure (5, a) shows $(\alpha h\upsilon)^2$ versus (hυ) plots of V_2O_3 thin films. By extrapolating the linear portions of the plots of $(\alpha h\upsilon)^2$ versus $h\upsilon$ to $\alpha h\upsilon = 0$ the E_g values were obtained.

According to Urbach law the width of localizes states E_u, can be determined from the formula (Urbach F, 1953: Ali H, 2005);

$$\alpha = \alpha_o \exp(h\upsilon/E_u) \qquad (10)$$

where, α_0 is a constant and E_u is the Urbach energy that gives the tail width of localized states in the optical band gap region. E_u values were determined from the slopes of the linear portions of Ln α vs. hυ plots as depicted in Figure (5, b). The average values of the absorption coefficient $\alpha_{avg.}$ in the visible spectral range, the optical band gap energy E_g and the width of localizes states E_u of V_2O_3 films are recorded in Table 2.

Figure 6 gives the spectral dependence of the refractive index n and extinction coefficient k that were calculated for different film thicknesses. As shown n and k values are almost the same of the tow thickness. n values in the Vis spectral range are relatively high (varying from 2 to 4), on the other hand k values are relatively low (varying from 0.03 to 0.05) these n and k values making these samples desirable for solar absorbers.

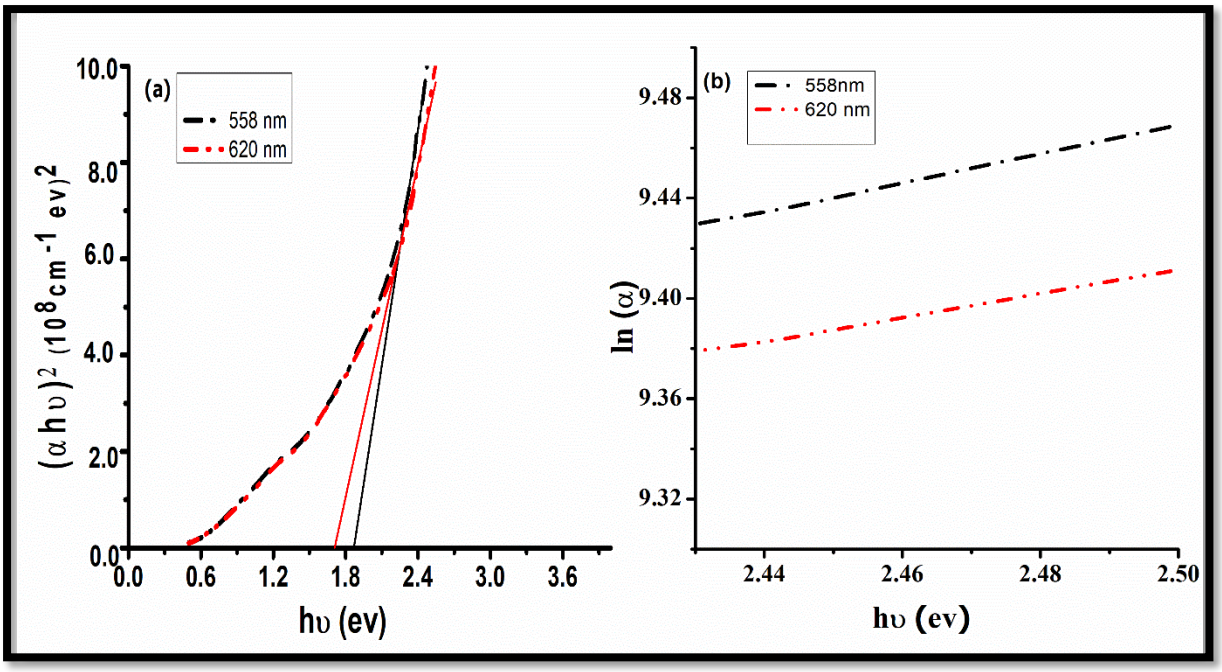

Figure 5: $(\alpha hv)^2 vs. hv$ (a) and $\ln \alpha \, vs. hv$ (b) plots for V_2O_3 thin films of 558 and 620 nm thick

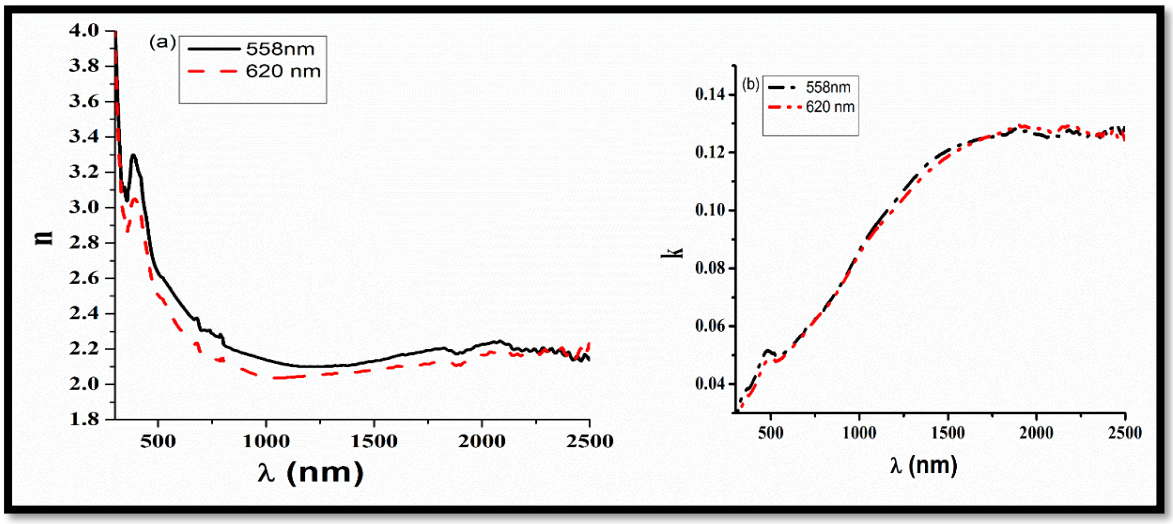

Figure 6: the spectral wavelength dependence of the refractive index and (a) the extinction coefficient (b) of V_2O_3 thin films of 558 and 620 nm thick.

According to Lark-Korovitz et al (Johnson et al., 2013). semiconductor samples of high carrier concentrations (extrinsic semiconductor materials) show variations of reflectivity at long wavelengths, where the free carrier contributes to the electrical susceptibility and conductivity (Becker M., 1951). The optical constants obtained from the samples can be used to find the electrical susceptibility of free carries, and consequently the high frequency dielectric constant. Spitzer and Fan (Verscharen et al., 2021) have shown that the contribution from the free carrier electrical susceptibility (χ_C) to the real dielectric constant (or lattice dielectric constant), can be given by the following equation (El-Nahass et al., 2004),

$$\epsilon^{/} = n^2 - k^2 = \epsilon_\infty - \left(\frac{1}{4}\epsilon_o\right)\left(\frac{e^2}{\pi c^2}\right)\left(\frac{N}{m^*}\right) = \epsilon_\infty + 4\pi\chi_c \qquad (11)$$

, where ε_∞ is the infinitely high frequency dielectric constant, N/m* is the ratio of carrier concentration to the effective mass, e is the electronic charge, c is the light velocity. By plotting $\acute{\varepsilon}$ against λ^2 and fitting a straight line, ε_∞ can be determined directly from the intercept on the vertical axis and (N/m*) can be determined from the slope as shown in Figure 7. The wavelength of plasma oscillations, which is the value of λ when $\acute{\varepsilon}$=0, can be calculated by

$\lambda_p = \sqrt{\frac{\varepsilon\infty}{slope}}$ and consequently the plasma frequency $\omega_p = \frac{2\pi c}{\lambda p}$ can be determined.

The dielectric parameters ε_∞, N/m, χ_C, λ_p and ω_P for V_2O_3 thin films of 558 and 620 nm thick are listed in Table 2. The calculated free carrier concentration shows that these samples are extrinsic semiconductors, where N/m values are in the range of $2.4x10^{21}$ - $4.4\ x10^{21}\ cm^{-3}$ when the film thickness increases from 558 to 620 nm, respectively. Also, χ_C and ω_P increases, but λ_p decreases with increasing the thickness.

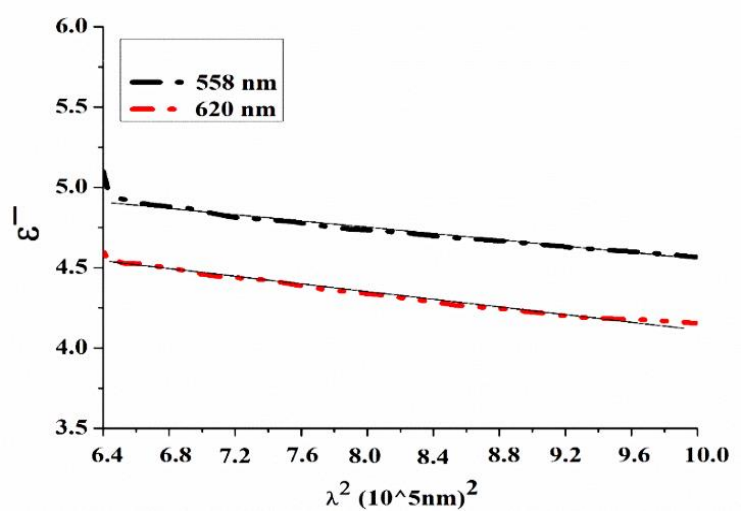

Figure 7: plots of $\varepsilon^{/} vs. \lambda^2$ for V_2O_3 thin films of 558 and 620 nm thick.

Table 2: *effect of thickness on E_g, E_u, $\alpha_{avg.}$ and the dielectric parameters of vanadium oxide thin films deposited by sol gel method on glass substrate.*

Thickness (nm)	***Eg (ev)***	***Eu (ev)***	***$\alpha_{avg.}$x10^4 cm^{-1}***	***Lattice dielectric constant =(ε_∞)***	***N/m, 10^{21} (cm^{-3})***	***λ_p,10^3 (nm)***	***ω_p, 10^{15} (sec)$^{-1}$***	***χ_c***
558	1.82	1.98	1.16	7.22	2.44	1.815	8.14	0.57
620	1.81	2.44	1.164	7.7	4.42	1.394	8.82	0.61

3.3 thermoelectric properties:

The thermoelectric measurements of V_2O_3 thin films of 558 and 620 nm thick have shown that the sign of Seebeck coefficient is positive, and there values are 85.7 & 104.3 μ *Volt/* ^{0}*C,* re-

spectively, this matching with other reported works (Hu L et al., 2020: Aksit et al., 2014: Wei et al., 2014: Yuan et al., 2018: Wei et al., 2018: Hu L et al., 2019), which have found that Seebeck coefficient has a positive value of V_2O_3 thin films and are p-type semiconductors or p-type metal with high intrinsic carrier concentration (Hu L et al., 2020).

All previously studied optical and thermoelectric properties of relatively thick V_2O_3 films refer to the ability to use these samples as a p-type absorber layer in solar cell applications.

4. Examining V_2O_3 for thin film solar cell:

V_2O_3 thin film of 620 nm thick was examined as absorber layer in thin film solar cell with structure of ITO/CdS/V_2O_3/Mo/Glass as depicted in Figure 8:

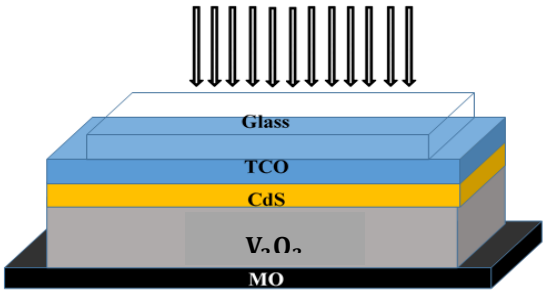

Figure 8: Schematic structures of thin-film solar cells based on V_2O_3 absorber.

The short-circuit current density, J_{sc}, was calculated with the use of the standard formula (Mohamed et al., 2018):

$$J_{SC} = q\sum_i T(\lambda)\frac{\Phi_i(\lambda_i)}{h\nu_i}\eta_{int}(\lambda_i)\Delta\lambda_i \qquad (12)$$

where Φ is the power density of the spectral radiation, $h\upsilon$ is the energy of the photon, $\Delta\lambda_i$ is the interval between values of the wavelength that are neighboring one another, and η_{int} is the internal quantum efficiency, which equals to the ratio between the generated electron-hole bears and the number of the absorbed photons. When $T(\lambda)=1$ and $\eta_{int}=1$, this means neglecting the optical and recombination losses.

According to the standard diode equation, the $J(V)$ characteristic of a single-junction solar cell under illumination can be written as the linear superposition of the dark characteristics of the cell and the photogenerated current:

$$J = J_d - J_{SC} = \left[exp\left(\frac{qv}{AkT}\right) - 1\right] - J_{SC} \qquad (13)$$

where J_d is the dark current, J_0 is the reverse saturation current, q is the elementary charge, k the Boltzmann constant, T the absolute temperature and A the idealist factor.

The solar cell efficiency η% was calculated from the numerical model according to the following equation (Mohamed et al., 2023).

$$\eta\% = \frac{FF\, J_{SC}\, V_{OC}}{P_{in}} \qquad (14)$$

where V_{oc} is the open-circuit voltage, FF is the fill factor and P_{in} is the input power (100 mW cm^{-2})

Accordingly, the calculated values of J_{SC} is about 19.43 mA/cm^2 as shown in Figure.9, the cell efficiency is 14.68% and the other cell parameters are listed in table 3.

The incident light can be lost due to the reflections between the solar cell layers and the absorption in ITO and CdS layers (optical losses). The reflection between any two layers is;

$$R_{12}(\lambda) = \frac{|n_1^* - n_2^*|^2}{|n_2^* + n_2^*|^2} = \frac{(n_1 - n_2)^2 + (k_1 - k_2)^2}{(n_1 + n_2)^2 + (k_1 + k_2)^2} \quad (15)$$

In this case, the transmitted light reaching the absorber layer (V_2O_3 layer) is given by;

$$T(\lambda) = (1 - R_{12})(1 - R_{23})(1 - R_{34}) \quad (16)$$

where R_{12}, R_{23} and R_{34} are the reflection at the interfaces of air/ITO, ITO/CdS, and CdS/V_2O_3, respectively.

Table 3: The short-circuit current density, J_{sc}, maximum voltage V_m, maximum current J_m, fill factor *FF* and cell efficiency η% of V_2O_3 solar cell.

$J_{sc}(mA/cm^2)$	$V_m(V)$	$J_m(mA/cm^2)$	$V_{OC}(V)$	*FF*	$\eta(\%)$
19.43	*0.76*	*19.32*	*0.85*	*0.89*	*14.68*
13.25	*0.75*	*12.62*	*0.83*	*0.87*	*9.59*
6.23	*0.75*	*5.6*	*0.81*	*.83*	*4.3*

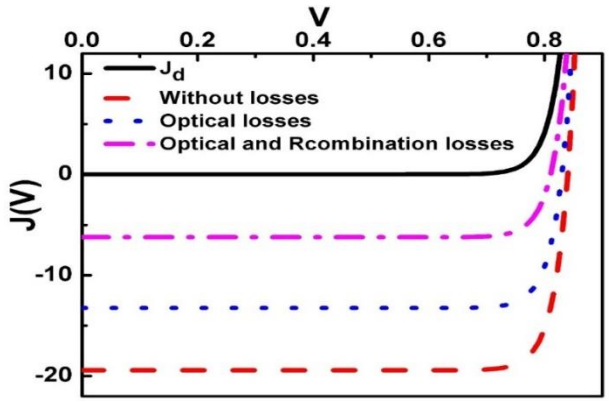

Figure 9: The dark current (J_d) and short-circuit current density (J_{sc}) in the case of both optical losses and recombination losses.

When the absorption takes place in ITO and CdS layers, equation (16) takes the following form (Mohamed et al., 2023):

$$T(\lambda) = (1 - R_{12})(1 - R_{23})(1 - R_{34})e^{-\alpha_1 d_1}e^{-\alpha_2 d_2} \quad (17)$$

where α_1 and α_2 are the absorption coefficients of ITO and CdS, respectively, and d_1(60 nm) and d_2 (100 nm) are their thicknesses.

By substituting Eq.17 into Eq.12, and considering η_{int} =1, the optical loss can be calculated. Literature data (Mohamed et al., 2018: Mohamed et al., 2023: Ninomiya& Adachi, 1995: Benmir& Aida, 2016: Gorji, 2014: Mohamed, 2015) were used to determine the values of *n* and *k* for ITO, CdS. Where, *n* and *k* values of V_2O_3 layer were taken from Figure 6. In this aspect, J_{SC} is about 13.3 mA/cm^2, and the cell efficiency is 9.6% as shown in Figure.9 and listed in table 3.

As can be seen, the small efficiency value obtained is mainly due to the use of a small thickness of the absorbing layer, and it appears that this thickness is not sufficient to absorb the entire incident light on the cell. On the other hand, this leads to an effective loss due to recombination of the photogenerated carriers. Under the effect of both the optical and recombination

losses, J_{SC} decreased dramatically and reached 6.23 mA/cm^2 and the corresponding cell efficiency is about 4.3%.

5. Conclusion.

V_2O_3 thin films were deposited sol-gel spin coating on glass and Si substrates and examined by XRD, SEM, EDAX, and UV/Vis/NIR spectroscopy. The crystallographic structure and EDAX analysis indicated that the deposited samples by the sol-gel technique are monoclinic V_2O_3 thin films. SEM analysis revealed the high surface homogeneity with grains size in micro-meter scale. The optical band gap energy of V_2O_3 thin films was found to be 1.82 & 1,.8 eV for thickness 558 and 620 nm, respectively and the localized state width increases from 1.9 to 2.44 eV.

The relatively high average values of absorption coefficient 1.16×10^4 cm^{-1} in the visible spectral range, besides the positive Seebeck coefficient (104.3 μV/°C) for the film of 620 nm thick qualify this sample to be used as an absorber layer un thin-film solar cells. In this work, the solar cell with the structure ITO/CdS/V_2O_3/Mo/Glass has been accomplished. It was found that the short circuit current density (J_{sc}) and the solar cell efficiency (η) in the absence of optical and recombination losses are 19.4(mA/cm^2) & 14.68 %, respectively. When the optical losses are taken into consideration, J_{sc} and η recorded the values of 13.3(mA/cm^2) & 9.6 %, respectively. Finaly when both the optical and recombination losses were affected in the cell, the values of J_{sc} and η decreased and reached to 6.23(mA/cm^2) & 4.2 %, respectively.

6. References:

Alamgir MK, Khan MZ, Ahmed RH, Razzaq. (2018). H. V _2 O _5 V 2 O 5 Thin Films Deposited by Sol–Gel and Indigenously Developed Spin Coating System. *Arabian Journal for Science and Engineering*. ;**43**:407-13.

Raj DV, Ponpandian N, Mangalaraj D, Viswanathan C.(2013). Effect of annealing and electrochemical properties of sol–gel dip coated nanocrystalline V2O5 thin films. *Materials Science in Semiconductor Processing*.;**16**(2):256-62.

Raja S, Bheeman D, Rajamani R, Bellan C. (2016). Structural and optical properties of vacuum evaporated V2O5 thin films. *Optik*.**127**(1):461-4.

Zou C, Rao Y, Alyamani A, Chu W, Chen M, Patterson DA, Emanuelsson EA, Gao W. (2010). Heterogeneous lollipop-like V2O5/ZnO array: a promising composite nanostructure for visible light photocatalysis. *Langmuir*. **26**(14):11615-20.

Mouratis K, Tudose V, Romanitan C, Pachiu C, Tutunaru O, Suchea M, Couris S, Vernardou D, Emmanouel K. (2020). Electrochromic performance of V2O5 thin films grown by spray pyrolysis. *Materials*. **13**(17):3859.

Gao L, Wang X, Fei L, Ji M, Zheng H, Zhang H, Shen T, Yang K. (2005) Synthesis and electrochemical properties of nanocrystalline V2O5 flake via a citric acid-assistant sol–gel method. *Journal of crystal growth*. **281**(2-4):463-7.

Benmouss M, Outzourhit A, Jourdani R, Bennouna A, Ameziane E. (2003). Structural, optical and electrochromic properties of sol–gel V 2 O 5 thin films. *Active and passive electronic components*. **26**:245-56.

Ozer N, Lampert C. (1999). Electrochromic performance of sol-gel deposited WO3–V2O5 films. *Thin solid films*. **349**(1-2):205-11.

Özer N. (1997). Electrochemical properties of sol-gel deposited vanadium pentoxide films. *Thin Solid Films*. **305**(1-2):80-7.

Shimizu Y, Nagase K, Miura N, Yamazoe N. (1990). New preparation process of V2O5 thin film based on spin-coating from organic vanadium solution. *Japanese Journal of applied physics*. **29** (9A):L1708.

Nagase K, Shimizu Y, Miura N, Yamazoe N. (1992). Electrochromic properties of vanadium pentoxide thin films prepared by new wet process. *Applied physics letters*. **60**(7):802-4.

Partlow D, Gurkovich S, Radford K, Denes L. (1991). Switchable vanadium oxide films by a sol-gel process. *Journal of Applied Physics*. **70**(1):443-52.

Hirashima H, Sudoh K. (1992). Preparation of V2O5 aerogels and aerogel coatings. *Journal of non-crystalline solids*. **145**:51-4.

El Mandouh Z, Selim M. (2000). Physical properties of vanadium pentoxide sol gel films. *Thin Solid Films*. **371**(1-2):259-63.

Huotari J. (2018). Vanadium oxide nanostructures and thin films for gas sensor applications.

Henrich VE, Cox PA. (1994). *The surface science of metal oxides*: Cambridge university press.

Pedrosa P, Cote J-M, Martin N, Arab Pour Yazdi M, Billard A. (2017). In situ electrical resistivity measurements of vanadium thin films performed in vacuum during different annealing cycles. *Review of Scientific Instruments*. **88**(2). https://doi.org/10.1063/1.4974847

Surnev S, Ramsey M, Netzer F. (2003). Vanadium oxide surface studies. *Progress in surface science*. **73**(4-8):117-65.

Ali HM, Hakeem AMA. (2015). Characterization of n and p-type (SnO2) x (ZnO) 1-x nanoparticles thin films. *The European Physical Journal Applied Physics*. **72**(1):10301.

Atuchin V, Ayupov B, Kochubey V, Pokrovsky L, Ramana C, Rumiantsev YM. (2008). Optical properties of textured V2O5/Si thin films deposited by reactive magnetron sputtering. *Optical Materials*. **30**(7):1145-8.

Tong Z, Li N, Lv H, Tian Y, Qu H, Zhang X, Zhao J, Li Y. (2016). Annealing synthesis of coralline V2O5 nanorod architecture for multicolor energy-efficient electrochromic device. *Solar Energy Materials and Solar Cells*. **146**:135-43.

Wang H, Yi X, Chen S, Fu X. (2005). Fabrication of vanadium oxide micro-optical switches. *Sensors and Actuators A: Physical*. **122**(1):108-12.

Shen K, Yang R, Wang D, Jeng M, Chaudhary S, Ho K, Wang D. (2016). Stable CdTe solar cell with V2O5 as a back contact buffer layer. *Solar energy materials and solar cells*. **144**:500-8.

Ramana C, Hussain O, Uthanna S, Naidu BS. (1998). Influence of oxygen partial pressure on the optical properties of electron beam evaporated vanadium pentoxide thin films. *Optical Materials*. **10**(2):101-7.

Park YJ, Ryu KS, Park N-G, Hong Y-S, Chang SH. (2002). RF-sputtered vanadium oxide films: Effect of film thickness on structural and electrochemical properties. *Journal of The Electrochemical Society*. **149**(5):A597.

Wu Q-H, Thissen A, Jaegermann W, Liu M. (2004). Photoelectron spectroscopy study of oxygen vacancy on vanadium oxides surface. *Applied Surface Science*. **236**(1-4):473-8.

Pan J, Li M, Luo Y, Wu H, Zhong L, Wang Q, Li G. (2016). Microwave-assisted hydrothermal synthesis of V2O5 nanorods assemblies with an improved Li-ion batteries performance. *Materials Research Bulletin*. **74**:90-5.

Song H, Zhang C, Liu Y, Liu C, Nan X, Cao G. (2015). Facile synthesis of mesoporous V2O5 nanosheets with superior rate capability and excellent cycling stability for lithium ion batteries. *Journal of Power Sources*. **294**:1-7.

Ihsan M, Meng Q, Li L, Li D, Wang H, Seng KH, Chen Z, Kennedy SJ, Guo Z, Liu H-K. (2015). V2O5/mesoporous carbon composite as a cathode material for lithium-ion batteries. *Electrochimica Acta*. **173**:172-7.

Niu C, Li J, Jin H, Shi H, Zhu Y, Wang W, Cao M. (2015). Self-template processed hierarchical V2O5 nanobelts as cathode for high performance lithium ion battery. *Electrochimica Acta*. **182**:621-8.

Sel S, Duygulu O, Kadiroglu U, Machin NE. (2014). Synthesis and characterization of nano-V2O5 by flame spray pyrolysis, and its cathodic performance in Li-ion rechargeable batteries. *Applied surface science*. **318**:150-6.

Libessart L, Djelal C, de Caro P. (2014). Influence of the type of release oil on steel formwork corrosion and facing aesthetics. *Construction and Building Materials*. **68**:391-401.

Rusop M, Uma K, Soga T, Jimbo T. (2006). Post-growth annealing of zinc oxide thin films pulsed laser deposited under enhanced oxygen pressure on quartz and silicon substrates. *Materials Science and Engineering: B*. **127**(2-3):150-3.

Mohamed HA-H, Ali HM. (2008). Characterization of ITO/CdO/glass thin films evaporated by electron beam technique. *Science and Technology of Advanced Materials*.

Wang X, Cui F, Lin J, Ding B, Yu J, Al-Deyab SS. (2012). Functionalized nanoporous TiO2 fibers on quartz crystal microbalance platform for formaldehyde sensor. *Sensors and Actuators B: Chemical*. **171**:658-65.

Long S, Cao X, Sun G, Li N, Chang T, Shao Z, Jin P. (2018). Effects of V2O3 buffer layers on sputtered VO2 smart windows: Improved thermochromic properties, tunable width of hysteresis loops and enhanced durability. *Applied Surface Science*. **441**:764-72.

Subramanian S, Padiyan DP. (2008). Effect of structural, electrical and optical properties of electrodeposited bismuth selenide thin films in polyaniline aqueous medium. *Materials Chemistry and Physics*. **107**(2-3):392-8.

Benramdane N, Murad W, Misho R, Ziane M, Kebbab Z. (1997). A chemical method for the preparation of thin films of CdO and ZnO. *Materials Chemistry and Physics*. **48**(2):119-23.

Saleh MH, Jafar MMA-G, Bulos BN, Al-Daraghmeh TM. (2014). Determination of optical properties of undoped amorphous selenium (a-Se) films by dielectric modeling of their normal-incidence transmittance spectra. *Applied Physics Research*. **6**(6):10. http://dx.doi.org/10.5539/apr.v6n6p10

Urbach F. (1953). The long-wavelength edge of photographic sensitivity and of the electronic absorption of solids. *Physical review*. **92**(5):1324.

Ali H. (2005). Characterization of a new transparent-conducting material of ZnO doped ITO thin films. *physica status solidi (a)*. **202**(14):2742-52.

Johnson VA. (2013).*Men of Physics: Karl Lark-Horovitz: Pioneer in Solid State Physics*: Elsevier.

Becker M. (1951). The Infrared Optical Properties of Silicon and Germanium: Purdue University.

Verscharen D, Wicks RT, Alexandrova O, Bruno R, Burgess D, Chen CH, D'amicis R, De Keyser J, de Wit TD, Franci L. (2021). A case for electron-astrophysics. *Experimental Astronomy*. 1-47. https://link.springer.com/article/10.1007/s10686-021-09761-5

El-Nahass M, Farag A, Ibrahim E, Abd-El-Rahman S. Structural. (2004). optical and electrical properties of thermally evaporated Ag2S thin films. *Vacuum*. **72**(4):453-60.

Hu L, Wei R, Tang X, Lu W, Zhu X, Sun Y. (2020). Design strategy for p-type transparent conducting oxides. *Journal of Applied Physics*. **128**(14).

Aksit M, Kolli S, Slauch I, Robinson RD. (2014). Misfit layered Ca3Co4O9 as a high figure of merit p-type transparent conducting oxide film through solution processing. *Applied Physics Letters*. **104** (16). https://doi.org/10.1063/1.4871506.

Wei R, Tang X, Hu L, Hui Z, Yang J, Luo H, Luo X, Dai J, Song W, Yang Z. (2014). Transparent conducting p-type thin films of c-axis self-oriented Bi 2 Sr 2 Co 2 O y with high figure of merit. *Chemical Communications*. **50**(68):9697-9.

Yuan D, Wang J, Fu N, Wu X, Ma Y, Wang S. (2018). Transparent conducting properties of c-axis-oriented Na x CoO 2 epitaxial thin films. *Science China Physics, Mechanics & Astronomy*. **61**:1-4.

Wei R, Zhang L, Hu L, Tang X, Yang J, Dai J, Song W, Zhu X, Sun Y. (2018). p-type transparent conductivity in high temperature superconducting Bi-2212 thin films. *Applied Physics Letters*. **112**(25).

Hu L, Zhao M, Liang S, Song D, Wei R, Tang X, Song W, Dai J, He G, Zhang C. (2019). Exploring high-performance p-type transparent conducting oxides based on electron correlation in V 2 O 3 thin films. *Physical Review Applied*. **12**(4):044035.

Mohamed H, Mohamed A, Ali H. (2018). Theoretical study of ZnS/CdS bi-layer for thin-film CdTe solar cell. *Materials Research Express*. **5**(5):056411.

Mohamed H, Taya Y, Ali SS, Mohamed W. (2023). Optical and electrical modeling of CZTSSe based thin-film solar cells. *Physica Scripta*. **98**(8):085516.

Ninomiya S, Adachi S. (1995). Optical properties of wurtzite CdS. *Journal of Applied Physics*. **78**(2):118390.

Benmir A, Aida MS. (2016). Simulation of a thin film solar cell based on copper zinc tin sulfo-selenide Cu2ZnSn (S, Se) 4. *Superlattices and Microstructures*. **91**:70-7.

Gorji NE. (2014). Quantitative analysis of the optical losses in CZTS thin-film semiconductors. *IEEE Transactions on Nanotechnology*. **13**(4):743-8.

Mohamed H. (2015). Optimized conditions for the improvement of thin film CdS/CdTe solar cells. *Thin Solid Films*. **589**:72-8.